Signature of Avalanche in Solar Flares as Measured by Photospheric Magnetic Fields

V.I. Abramenko
Big Bear Solar Observatory, 40386 N. Shore Lane, Big Bear City, CA 92314, USA
Crimean Astrophysical Observatory, 98409, Nauchny, Crimea, Ukraine

and

V.B. Yurchyshyn, H. Wang, T.J. Spirock, P. R. Goode
Big Bear Solar Observatory, 40386 N. Shore Lane, Big Bear City, CA 92314, USA

ABSTRACT

Turbulent/fractal parameters of the longitudinal magnetic field, B_z, for four powerful solar flares were analyzed utilizing the correlation length, λ, of the magnetic energy dissipation field and the scaling exponent, β, which characterizes the measure of intermittency of the B_z structure. We select a set of four two-ribbon flares, which were followed by coronal mass ejections, for the study of magnetic structure. During the course of each flare, we found a peak in β which was followed by a peak in λ in all of the cases studied in this paper. These two peaks were separated by the time interval τ_λ during which a rapid growth of the soft X-ray and $H\alpha$ flux occurred. The peak in β was preceded by a time period τ_β during which β increased gradually. For all of the flares τ_β was longer than the time interval τ_λ. The maximum of λ occurred nearly simultaneously, within an accuracy of about 2-5 minutes, with the maximum of the hard X-ray emission. For the four flares considered in this paper, we concluded that the more impulsive and/or more powerful a flare is, the shorter the β growth time, τ_β, and the λ growth time, τ_λ, are. In the framework of the theory of non-linear dissipative processes, these results may be interpreted as follows. Before a solar flare occurs there is a significant increase in the number of magnetic field discontinuities (β increasing), which is followed by an avalanche (increase of the correlation length) of magnetic energy dissipation events. The avalanche event occupies the entire active region from the corona to the photosphere. Our study indicates that the more abrupt is the avalanche, the stronger and/or more impulsive a flare is. The time profiles of an avalanche is either Gaussian, which satisfies the logistic avalanche model, or exponential with an abrupt drop, which satisfies the exponential avalanche model. The

driving time, τ_β, was longer than the avalanching time, τ_λ, for all of the events. This qualitatively agrees with the requirements of the self-organized criticality theory.

Subject headings: Sun: magnetic fields; flares; avalanches

1. Introduction

It is well known that magnetic reconnection is the mechanism responsible for the release of magnetic energy which causes solar flares. According to Parker's conjecture (Parker, 1983, 1988), a solar flare can be considered to be a cluster of nanoflares - an aggregate of small-scale energy release events occurring as a result of reconnection processes at numerous tangential discontinuities. These discontinuities arise, in turn, as a consequence of the random motions of footpoints of magnetic loops in the photosphere and/or the emergence of twisted and braided magnetic flux tubes (Leka et al.1996, Wang and Abramenko 2000).

By the mid 80's, it had been determined that the energy distribution of hard X-ray bursts in solar flares follows a power law (Datlow et al. 1974; Lin et al. 1984; Dennis 1985). In order to explain the statistical properties of solar flares in the framework of Parker's conjecture, Lu and Hamilton (1991) suggested that the solar magnetic field is in a state of self-organized criticality (SOC) and, therefore, that a flare is the collective energy released by an avalanche of reconnection events. A system in a state of SOC displays a scaling behavior which can be described by a spatial and temporal power law. Since the first publication on this subject (Lu and Hamilton 1991), the idea that the non-linear dynamical evolution of the flaring corona is governed by scale-invariant statistics, has gained much favor. In particular, a voluminous body of literature has been devoted to improving the theoretical and computational aspects of the SOC-model (Vlahos et al. 1995; MacKinnon et al. 1996; Longcope and Noonan 2000; Norman et al. 2001; McIntosh and Charbonneau 2001; Krasnoselskikh et al. 2002). Analysis of new observational data revealed new aspects where power laws are valid for solar flare statistics (Aschwanden et al. 1998; Wheatland et al. 1998; Wheatland 2000; Georgoulis et al. 2001; Aschwanden and Parnell 2002).

In their recent review of avalanche models, Charbonneau and coauthors (2001) analyzed advantages and disadvantages of several modifications of the SOC-model and pointed out one aspect of the relation between the validity of a power law and a state of SOC that is not obvious: the former is not equivalent to the latter. The existance of power law distributions is a necessary, but not a sufficient condition, for the system to be in the SOC state. Thus, power laws themselves can not serve as strict proof that the system is in a state of SOC.

Generalization of the SOC concept was proposed by Aschwanden et al. (1998), which is based on the so-called logistic equation mathematical formalism and the analysis of elementary time structures of energy dissipation. Their logistic avalanche model does not require the presence of a SOC in order to provide the power laws and gives a more realistic avalanche profile without a discontinuity of the energy dissipation rate at the time of the avalanche maximum. Therefore, nonlinear energy dissipation processes produce avalanches of energy dissipation events (sudden growth of the energy dissipation rate followed by its decrease). As long as it is magnetic energy that dissipates in a solar flare, then certain signatures of avalanche events might be seen in the dissipation of magnetic energy in the course of a flare. (Note, that until now, the presence of avalanche events in solar flares has been inferred indirectly by power laws and directly by time series of X-ray and radio emissions). In the present study, we intend to clarify this question. Certain similarities between the nonlinear dissipation processes theory and the percolation theory gives us a guess as to how this can be done. An avalanche event in nonlinear energy dissipation processes corresponds to a state of percolation of a cluster in the percolation theory (Feder 1988, Pustil'nik 1998, Schroeder 2000). Namely, of the cluster of energy dissipation. Next, we will explain this idea in detail.

The easiest way to explain a state of percolation is to use a forest fire as an analogy (Schroeder 2000). For simplicity, let us represent a forest as a square point lattice in which trees independently occupy the lattice points with the probability $p < 1$ (p is equal to the total number of trees divided by the total number of lattice points). Let the lowest row of trees be ignited. We will assume that a burning tree will always ignite all of the trees located at adjacent grid points after one unite of time. If the probability p is below the critical value p_c, i.e. the total lattice space is only populated by few, widely spaced, trees, the fire will die out before reaching the other edge of the forest. On the contrary, if $p > p_c$ (there are many closely spaced trees), the fire will quickly spread and reach the far edge of the forest. In the state near the percolation threshold, when $p \approx p_c$, a characteristic size (i.e. a correlation length) of the cluster of the trees before the fire grows to the size of the entire lattice. In other words, continuous chains of trees can be drawn from the lowest row of trees to the highest. In such a situation, any ignited tree in the lowest row may start a fire which will spread quickly to the upper boundary. A cluster of burning trees is nothing more than a representation of the cluster of energy dissipation events. As the correlation length of the cluster before the fire increases to the size of the entire lattice, as when $p \longrightarrow p_c$, so does the correlation length of the energy dissipation cluster, because the fire can easily percolate through the continuous chains of trees. The maximum rate of energy release will be reached, evidently, at the moment of maximal characteristic size (or correlation length) of a dissipative cluster. This is a state of percolation.

Since solar flares are the result of magnetic energy dissipation,we have chosen to analyze a cluster of magnetic energy dissipation events.

Using measurements of the longitudinal magnetic field covering four major flares, we calculated the magnetic energy dissipation field, $\varepsilon(\mathbf{x})$, and the correlation length, λ. Variations of λ during the course of a flare were the focus of our study.

Along with the calculation of the correlation length, we also computed a scaling parameter, β, according to the formula published in Abramenko et al. (2002). Variations of β, during the course of a flare, reflect changes in the strength of the discontinuities in the magnetic field.

2. Observations

When we selected data for the purposes mentioned above, we used the following criteria. Namely, in order to reduce projection effects, we had to select only those active regions which were located near the central meridian (no more than 40 degrees away from the disk center).

The measurements should also cover time periods before, during and after a major flare (M-class and higher) with an appropriate time cadence and excellent seeing. For this purpose, we used the Big Bear Solar Observatory (BBSO) archive of magnetic field measurements acquired between 1991 and 2002. We selected four cases which satisfied all of the above requirements. The selected active regions are listed in Table 1 (in order of increasing X-ray class) and the corresponding longitudinal magnetograms are shown in Fig. 1.

Active regions NOAA 6555 and 8375 were observed with the BBSO videomagnetograph system (Varsik 1995). The dimension of the CCD array was 481×512 pixels and the scale of each pixel was $0''.76 \times 0''.60$. Observations for active regions NOAA 9661 and 0039 were carried out with the BBSO digital magnetograph system (Spirock et al. 2001) by a 512×512 CCD camera with a pixel scale of $0''.60 \times 0''.60$. All magnetograms were taken with the Ca I 6103Å spectral line.

We also used 1-8Å GOES X-ray data and BBSO full disk $H\alpha$ images. Unfortunately, for active region NOAA 6555 the later was not available.

All flares analyzed here were of the two-ribbon type and were followed by coronal mass ejections.

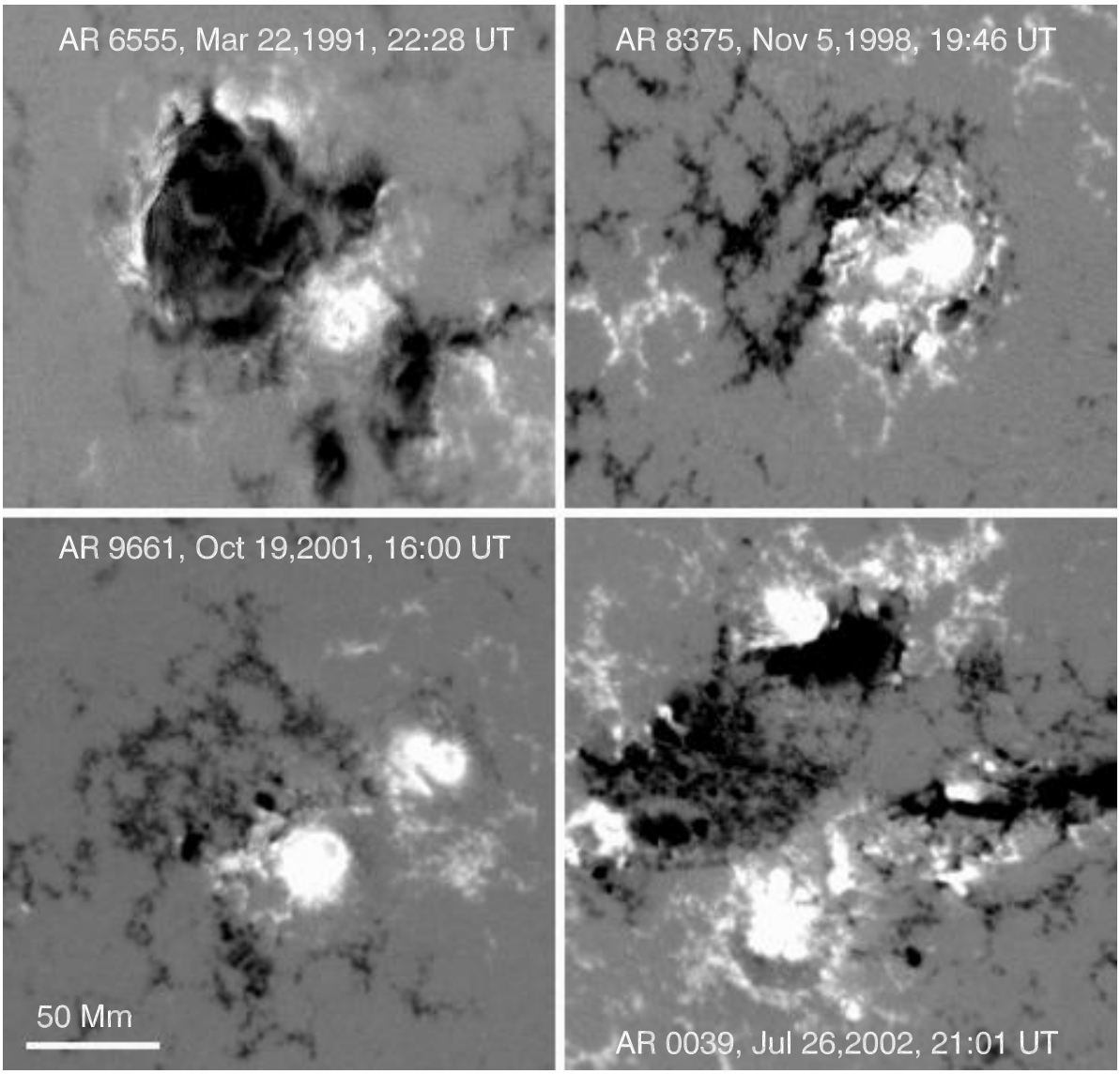

Fig. 1.— Maps of the longitudinal magnetic field of the four active regions under study. Images are scaled with a range of ±500 G. West is to the *right* and north is to the *top*.

The M8.4 flare, which occurred on November 5, 1998 in active region NOAA 8375, was analyzed, in detail, by Wang et al. (2000) and by Yurchyshyn et al. (2000). This was the only case, of the four flares considered in this study, when the seeing and instrumental conditions were very good for more than the two-hour period covering the entire flare. We used 94 magnetograms acquired between 18:54 and 20:54 UT in order to analyze the variations in λ and β.

For the M8.7 flare, in active region NOAA 0039 on July 26, 2002, the seeing conditions

allowed us to choose only 13 magnetograms covering a time interval of about 1 hour 15 minutes, which included the flare.

The X1.6 flare, on October 19, 2001 in active region NOAA 9661, was studied by Wang et al. (2002), where they payed special attention to variations in the magnetic flux and shear inside a small area which contained the brightest Hα kernels. Note, that in the present study, we analyzed parameters calculated over the entire active region. The 24 magnetograms of the highest quality were used.

The X9.4 flare, of cycle 22, occurred on March 22, 1991 in active region NOAA 6555. This event was discussed, in detail, by Wang and Tang (1993) and Wang et al. (2002). It was the most powerful, and impulsive, flare among the four analyzed in this paper. For this event, we only chose the 9 best magnetograms, covering a half-hour interval, centered on the flare maximum.

In order to follow the evolution of each solar flare, we used 1-8Å X-ray flux obtained from the GOES satellite and Hα flux data from BBSO full disk Hα observations. These data are shown in Figs. 4 – 7 (upper panels).

3. Methods

3.1. Correlation length of the magnetic energy dissipation field

For a turbulent system, the energy dissipation, per unit mass in a unit of time, is defined by Monin and Yaglom (1975) as:

$$\varepsilon(\mathbf{x}) = \frac{\nu}{2} \sum \left(\frac{du_i}{dx_j} + \frac{du_j}{dx_i} \right)^2 , \tag{1}$$

where ν is the viscosity coefficient.

To calculate the magnetic energy dissipation field in the photosphere using equation (1), one needs simultaneous measurements of the magnetic vector field inside a volume, which are not, as yet, available. For this reason, we will discuss the dissipation of the longitudinal component, B_z, of the photospheric magnetic field for which we can write

$$\varepsilon(B_z) = \nu_m \left(4 \left(\left(\frac{dB_z}{dx} \right)^2 + \left(\frac{dB_z}{dy} \right)^2 \right) + 2 \left(\frac{dB_z}{dx} + \frac{dB_z}{dy} \right)^2 \right) . \tag{2}$$

Assuming tha the magnetic viscosity, ν_m, is spatially uniform and equal to unity, we calculated the 2D magnetic energy dissipation, $\varepsilon(B_z)$, using equation (2). These structures,

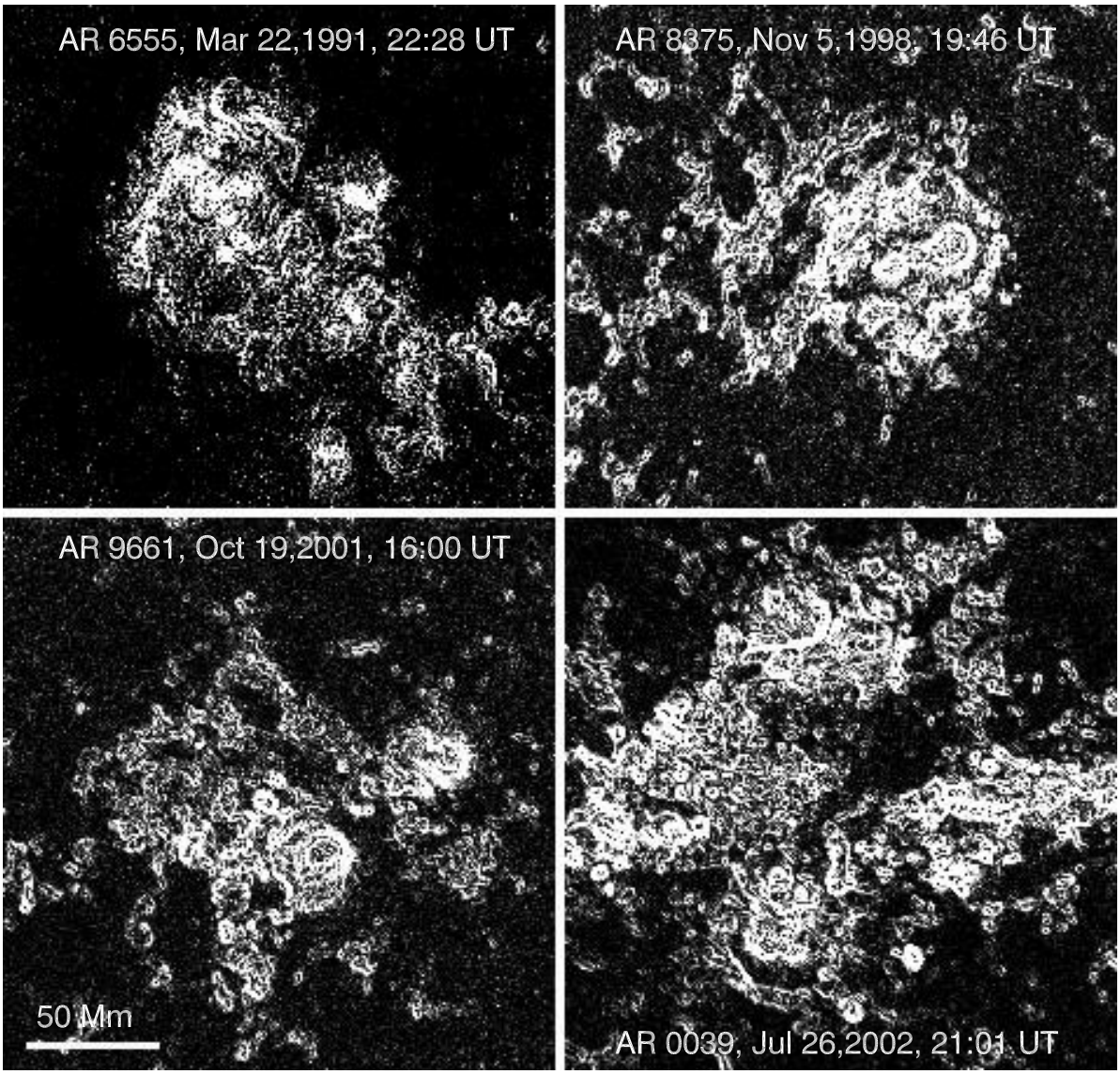

Fig. 2.— Structures of magnetic energy dissipation, $\varepsilon(B_z)$, shown in *arbitrary units*, were calculated by using eq. (2) for the magnetograms shown in Fig. 1

.

for each active region in this study, are shown in Fig. 2. One can see that these structures are very jagged and intertwined and resemble percolation clusters (Feder 1988). Our next aim is to define the correlation length of these clusters. Following Monin and Yaglom (1975), we used a method of the turbulence theory to calculate the correlation length of the energy dissipation field.

Let us first denote that $\varepsilon(B_z) = \varepsilon$. Then, we define a correlation function $B(r)$:

$$B(r) = \langle(\varepsilon(\mathbf{x}+\mathbf{r}) - \langle\varepsilon\rangle) \cdot (\varepsilon(\mathbf{x}) - \langle\varepsilon\rangle)\rangle, \tag{3}$$

where $\mathbf{r}$ is a separation vector and $\mathbf{x} \equiv (x, y)$ is the current point on a magnetogram. Angle brackets denote the average over the area.

In order to obtain a correlation length we have to normalize $B(r)$ by the variance of dissipation , $B(0)$:

$$b(r) = B(r)/B(0). \tag{4}$$

By integrating the normalized correlation function, $b(r)$, over all scales r, we obtain a correlation length of the energy dissipation field, λ, (Monin and Yaglom 1975):

$$\lambda = \int_0^{r_{max}} b(r)dr. \tag{5}$$

Note, that λ calculated by using equations (3), (4) and (5) does not depend on our assumption that $\nu_m = 1$.

Examples of $b(r)$, calculated from two magnetograms of active region NOAA 9661, are plotted in Fig. 3. One can see that the two curves are noticeably different and the difference in the area under the curves of $b(r)$ can not be neglected. Therefore, by calculating λ for a sequence of magnetograms, we can analyze its evolution.

3.2. Measure of intermittency of the magnetic field

According to Parker's conjuncture (Parker 1988), the intensity of tangential discontinuities of the magnetic field is reduced in the course of a solar flare. The higher the intensity of the discontinuities the more intermittent is the magnetic field (Parker 2002). One way to analyze the measure of intermittency of a turbulent field is to calculate its structure functions (Frisch 1995):

$$S_q(r) = \langle|B_z(\mathbf{x}+\mathbf{r}) - B_z(\mathbf{x})|^q\rangle \sim (r)^{\zeta(q)}. \tag{6}$$

Here, q is a real number, $\mathbf{r}$ is a separation vector, $\mathbf{x} \equiv (x, y)$ is the current point on a magnetogram and B_z is the observed longitudinal magnetic field. The rightmost expression in equation (6) holds in the inertial range separations.

For non-intermittent classical Kolmogorov's turbulence $\zeta(q) = q/3$ (Kolmogorov 1941), whereas, for highly intermittent turbulence, $\zeta(q)$ deviates from a straight $q/3$ line.

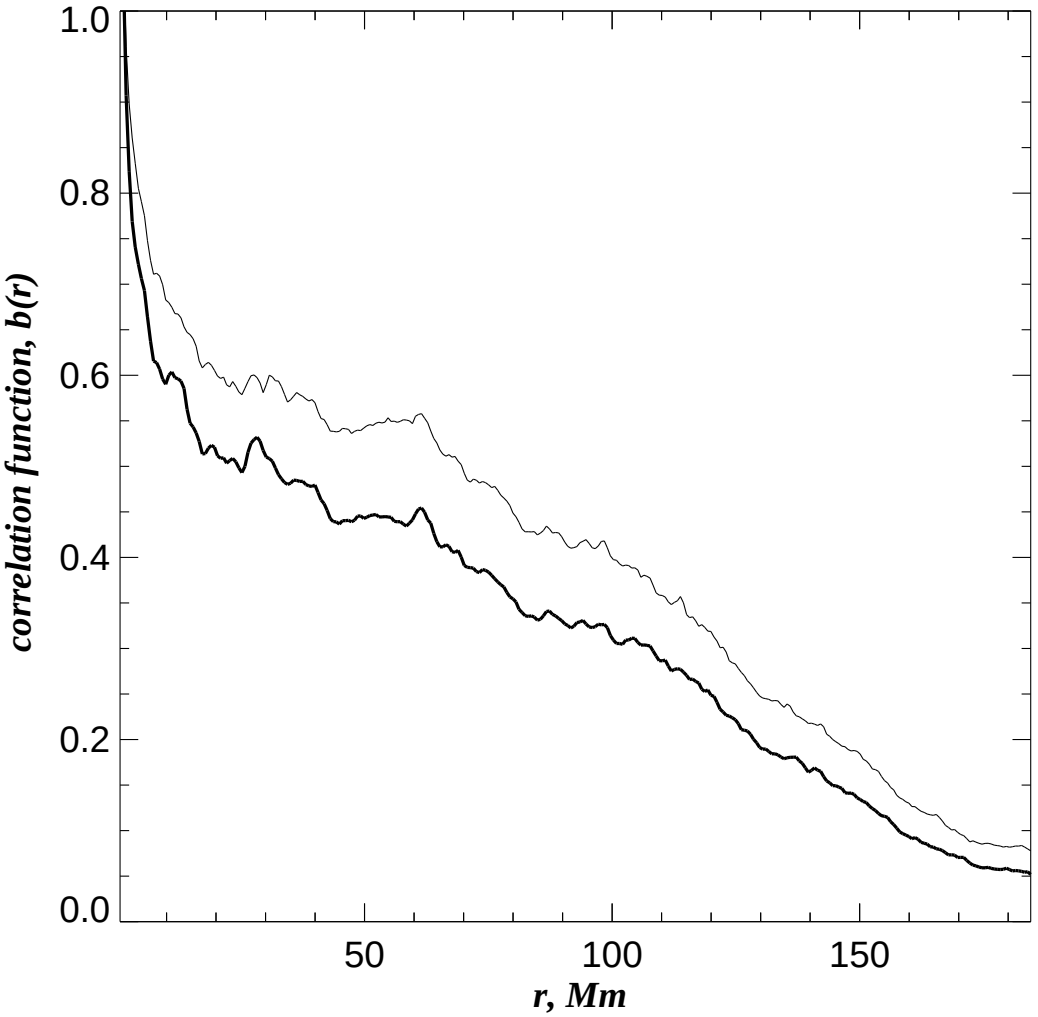

Fig. 3.— Plots of the normalized correlation function, $b(r)$, of magnetic energy dissipation calculated by using eqs. 3 and 4 for two magnetograms of active region NOAA 9661. The areas under the curves are equal to the correlation length λ of the magnetic energy dissipation at two different times. *The thick line* corresponds to the moment of the minimal correlation length near the beginning of the flare (16:19:37 UT). *The thin line* shows the correlation function when λ was at its maximum near the peak of the flare (16:27:04 UT).

The scaling behavior of structure functions in different applications was studied previously by many authors (Stolovitzky and Sreenivasan 1993; Vainshtein et al. 1994; She and Leveque 1994; Consolini et al 1999; see also a review by Frisch 1995). Recently, the scaling behavior of structure functions of solar magnetic fields was studied by Abramenko et al. (2002).

In general, the higher the value of q, used in the calculation of the structure functions, the more reliable is the diagnostics of intermittency. However, the upper limit for q is set by the number of nodal points, N, in the area under the study: $10^q \approx N$. With our data, we can estimate $\zeta(q)$ for all values of $q \leq 6$. For non-intermittent fields, $\zeta(6) \approx 2$, while it decreases in the case of highly intermittent structures (see Figs. 4 and 8 in Abramenko et al. 2002). After $\zeta(6)$ is calculated from the observed B_z, one can easily acquire a scaling exponent, β, of a power spectrum of magnetic energy dissipation (Abramenko et al. 2002) using:

$$\beta = 1 - \zeta(6). \tag{7}$$

Thus, β is close to -1 in the case of non-intermittent turbulence, and increases up to zero as the measure of intermittency rises (the strength of the discontinuities of magnetic field increases).

There are several numerical methods proposed to calculate β. In the present study, a self-similarity code (SS), described in Abramenko et al.(2002), was applied to three out of the four active regions. In the case of active region NOAA 9661, we were forced to use another method, namely, the extended self-similarity code (ESS, see Benzi et al. 1993; Briscolini et al. 1994, Consolini et al. 1999). This code allows the reduction of ambiguities caused by poor linearity of the spectrum $log(S_q(r))$ vs $log(r)$. According to our research, the ESS method produces values for β a bit lower when compared to the SS code. However, gradients in the time profile of β are the same. Values of β obtained by the ESS method for AR NOAA 9661 are denoted by stars in Fig. 6 and in Table 1.

4. Data processing and results

The main results of our study are presented in Figs. 4 – 7. The most important parameters are gathered in Tables 1 and 2, where the active regions are arranged in the order of increasing magnitude.

4.1. Magnetic flux changes and seeing variations

We would like to emphasize that parameters λ and β, discussed in section 3, are *structural* parameters of a 2D field. Therefore, they do not depend on a calibration coefficient or other uniform changes of the measured signal. It is not required to specify any thresholds for the calculation of these parameters (as opposed to the calculations of the fractal dimension). However, seeing variations may affect the values of λ and β. To reduce the influence of seeing, we only chose magnetograms of good quality for each active region. In order to control the quality of the data quantitatively, we calculated the image contrast as follows:

$$c = \sigma(\mid B_z \mid)/\langle \mid B_z \mid \rangle. \tag{8}$$

Here, $\sigma(\mid B_z \mid)$ is the standard deviation of the absolute value of the measured longitudinal magnetic field. The image contrast was calculated over areas located far from main sunspots. Variations of c, normalized to the value of c for the first magnetogram in a set, are shown in Figs. 4 – 7, (middle panels, squares).

To ensure that the longitudinal magnetic field measurements were carried out under steady instrumental conditions, the total positive, F^+, and total negative, F^-, magnetic flux over the entire magnetogram were calculated. Their time variations, normalized to the value of F^+ (F^-) of the first magnetogram in a set, are shown in Figs. 4 – 7, (middle panels, stars and triangles, respectively).

One can see that, in all of the cases during the time intervals under study, there were no drastic changes in the total magnetic flux or in the contrast.

Generally, during a strong flare, the measurements of the longitudinal magnetic field can be affected by changes in the spectral line profile due to photospheric heating in the region of the flare. However, a comprehensive investigation of such an effect requires high-cadence measurements of the Stokes profiles of the CaI 6103Å line during the flare, which are not yet available. Besides, only a small area of an active region is usually affected by changes in the line profile, namely, the area of the brightest Hα kernels. According to our study, possible distortions of the longitudinal magnetic field over a small fraction of the area of the entire active region does not noticeably change the values of λ and β, as long as they are computed by averaging over the entire active region (possible differences are within computational errors).

Comparison of the upper and middle panels of Figs. 4 – 7 shows that, from the beginning to the end of each flare, there were no correlated changes between the seeing and instrumental parameters (c, F^+, F^-,) with Hα and X-ray flux. This fact allows us to conclude that the changes in the magnetic field parameters, λ and β, which will be discussed

later in this paper, do not seem to be caused by seeing and instrumental problems.

Besides, as will be discussed shortly, we would like to note, that in two out of the four cases (the M8.4 and X9.4 flares, Figs. 4 and 7, respectively) the key changes in λ and β started *before* the beginning of the flares. That means that those changes were not caused by variations in the spectral line profile, which can arise only during a flare.

4.2. Proxy for Hard X-ray emission

It is well-known that there exists a temporal correlation between thermal soft X-ray emission and the integral of the nonthermal hard X-ray emission. This relation is called the Neupert effect and is based upon an assumption that all of the energy deposited by precipitating electrons is converted into heat in the chromosphere by trapping (Dennis and Zarro 1993; Veronig et al. 2002). Thus, the derivative of the soft X-ray emission, which displays the rate of its growth and/or decline, can, as well, serve as a proxy for the hard X-ray emission time profile. Note that the maximum of the hard X-ray emission is thought to coincide with the peak in the energy dissipation rate in the corona (Aschwanden et al. 1998).

In this paper we used the derivative of soft X-ray emission, which is shown in Figs. 4 – 7 (upper panels) in order to estimate the moments of the peaks in the energy dissipation rate in the corona. Hereafter, unless otherwise noted, the term HXR emission will refer to the time derivative of soft X-ray emission.

4.3. Variation of λ and β during a flare

The lower panels in Figs. 4 – 7 display the time variations of the correlation length, λ, of the magnetic energy dissipation and the scaling exponent, β, which characterizes a measure of intermittency (multifractality) of a B_z structure.

For the M8.4 and X1.6 solar flares, the cadence of the observations was sufficient to allow us to average the parameters by using 5 data points for the M8.4 flare and 3 data points for the X1.6 flare to calculate a running mean. Smoothed time profiles for λ and β are shown by bold lines in the bottom panels of Figs. 4 and 6. In this paper, for these two flares, the magnitude of the changes in λ and β were defined by the smoothed time profiles.

For each flare, we identified a time period, τ_β, when there was a gradual pre-flare increase in the parameter β. The left vertical dotted line in Figs. 4 – 7 marks the end of τ_β,

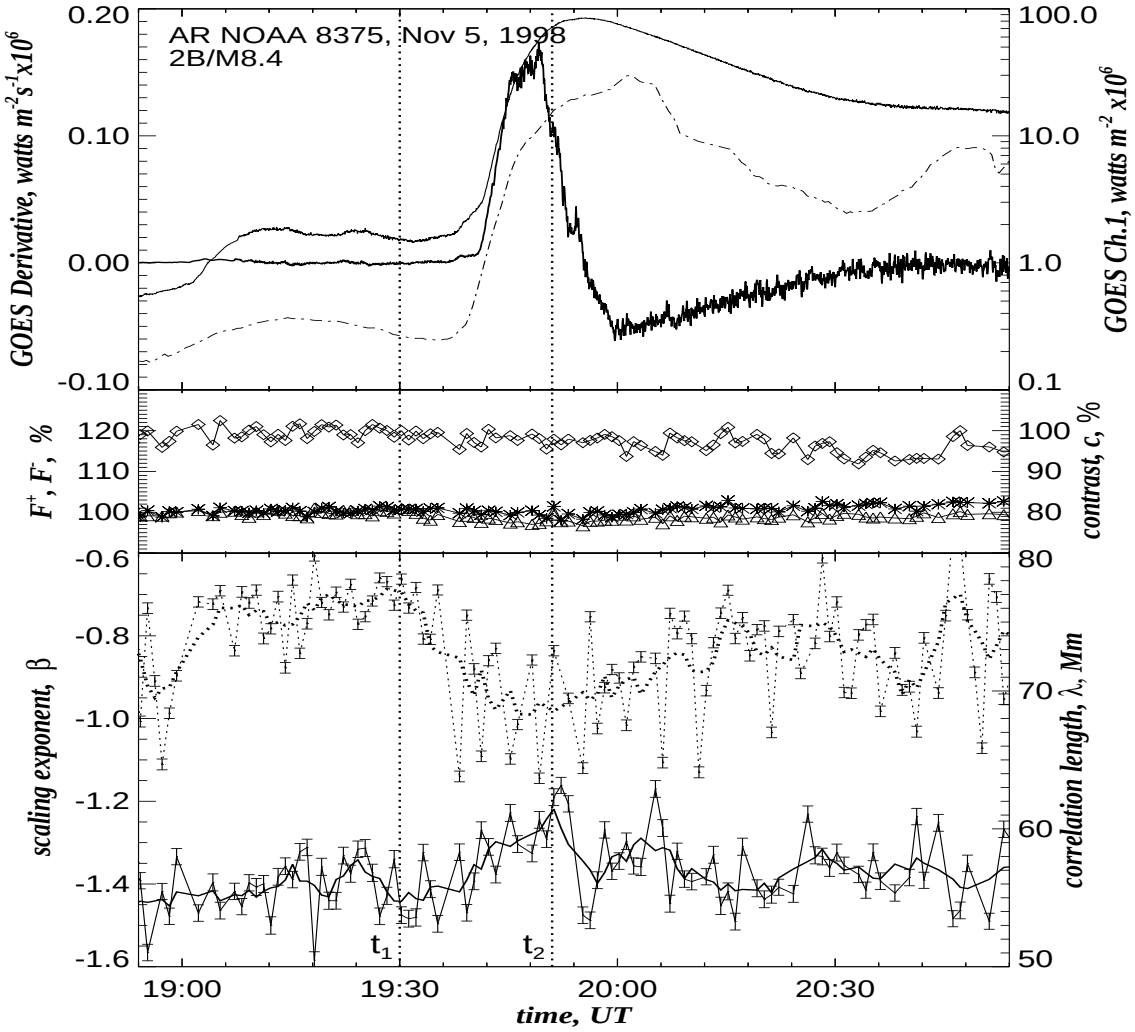

Fig. 4.— Time variations of parameters for the M8.4 flare on Nov 5, 1998 in AR NOAA 8375. *The upper panel* shows the 1 - 8Å GOES X-ray flux (*thin line, right axis*), its time derivative (a proxy for HXR emission, *thick line, left axis*) and the flux of Hα emission in arbitrary units (*dash-dotted line*). In *the middle panel* we plot the relative variations of contrast c (*diamonds, right axis*), total positive flux F^+ (*stars, left axis*) and total negative flux F^- (*triangles, left axis*). In *the bottom panel* we plot the variations of the correlation length (*solid lines*) and the scaling exponent β (*dotted lines*). *The thin lines* show their original values, calculated for each magnetogram, while *the thick lines* are their smoothed values. *The left vertical dotted line* marks the moment of maximum β, t_1. *The right vertical dotted line* indicates the moment, when λ is maximum, t_2. The time interval between the two vertical lines is defined as τ_λ (see text, Section 4.3).

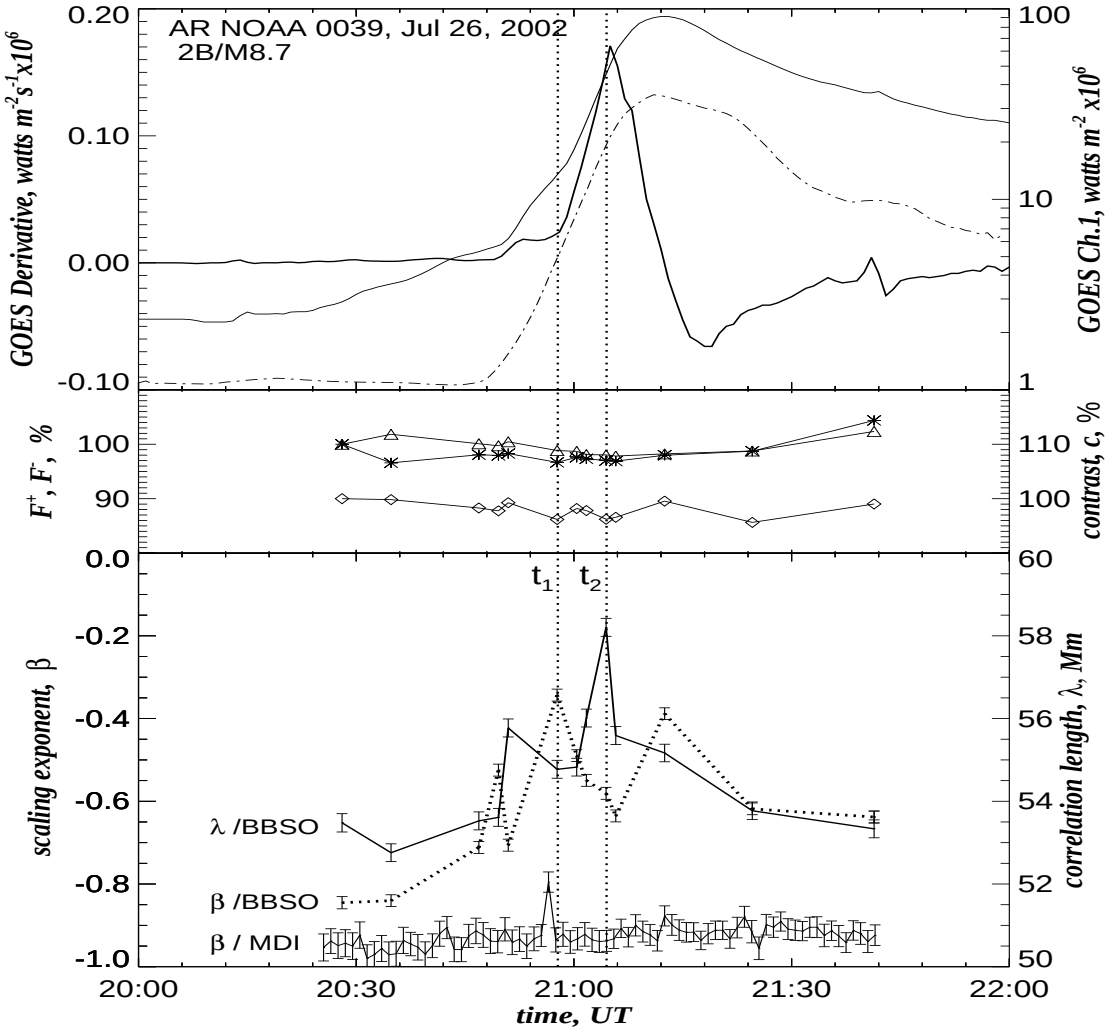

Fig. 5.— Time variations of parameters for the M8.7 flare on July 26, 2002 in active region NOAA 0039. The notations for *the top and middle panels* are the same as in Fig. 4. *The bottom panel* shows the non-smoothed values for the scaling exponent, β, (*dotted line*) and correlation length, λ, (*bold solid line*) calculated for each magnetogram. *The thin solid line* in the lower part of *the bottom panel* shows the values of β (*left axis*) calculated by using the full disk MDI magnetograms.

i.e. the moment, t_1, of maximum β and the beginning of its rapid decrease. For example, in the case of the M8.4 flare (Fig. 4), $\tau_\beta \approx 33$ minutes which lasted from 18:57 UT to t_1 =19:30 UT. In the 3rd column of Table 2, we list τ_β for all of the flares. We will define τ_β to be the growth time of β. The increase of β indicates the growth of the intermittency of B_z, i.e. the number of discontinuities in the magnetic field increases. This time interval

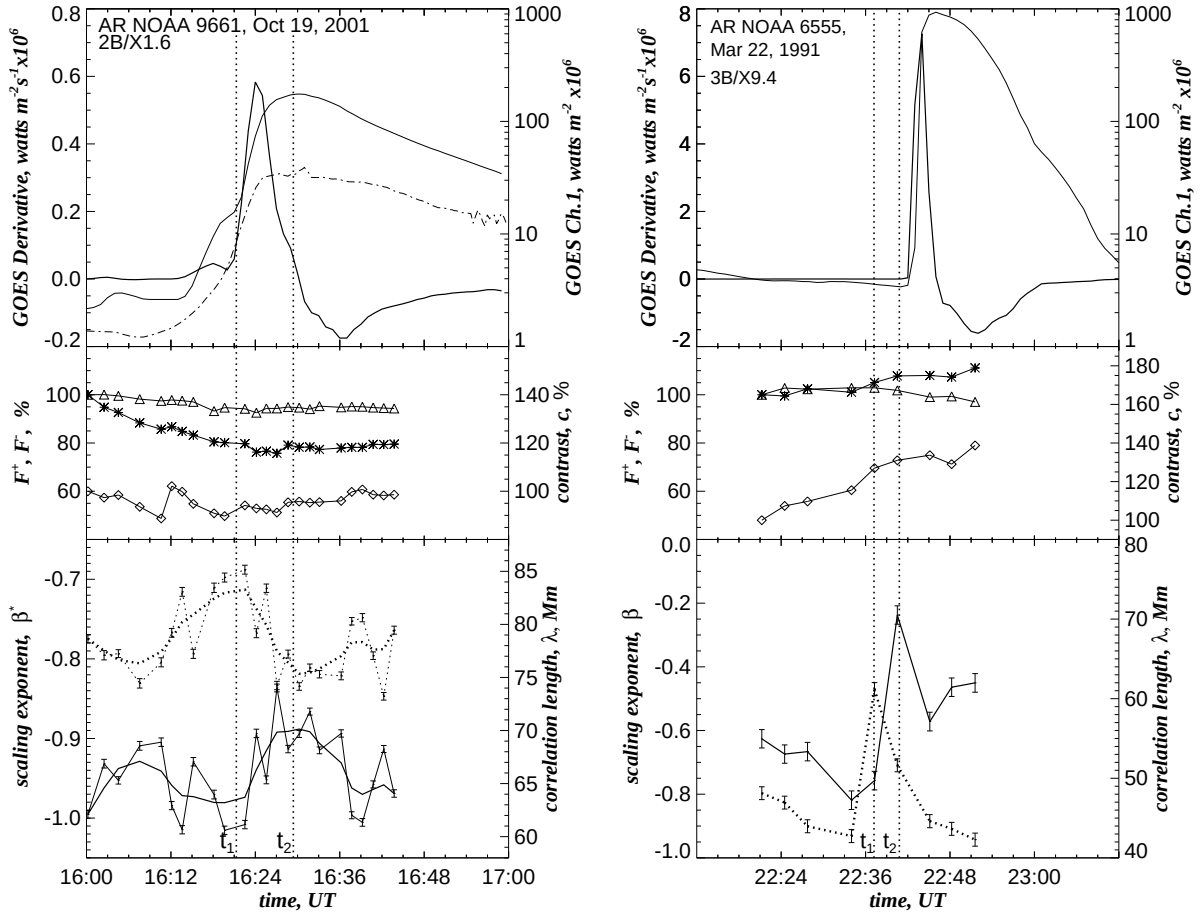

Fig. 6.— Time variations of parameters for the X1.6 flare on October 19, 2001 in active region NOAA 9661 . The notations are the same as in Fig. 4.

Fig. 7.— Time variations of parameters for the X9.4 flare on March 22, 1991 in active region NOAA 6555. The notations are the same as in Fig. 5.

can be considered to be a period of preflare small-scale rearrangements in the photospheric magnetic field.

The moment t_1 corresponds to the primary (over the period under study) maximum of β for all of the cases. To clarify the origin of the secondary maximum in β, at 20:12 UT in the case of AR 0039 (see Fig.5), we used full disk MDI magnetograms with a resolution of $4'' \times 4''$. The time profile of β as calculated from the MDI data is shown in Fig. 5 (bottom panel). The preflare peak in β is clearly visible. Due to the coarse spatial resolution (as compared to the BBSO data), the values of β are lower and the errors are larger.

Comparison between the β/MDI and the β/BBSO time profiles in Fig. 5 shows that the primary maximum in β occurred before t_1 and it was missed in the BBSO data due to the poor time resolution. This allows us to conclude that the real maximum value of β could be higher than -0.36, which was measured at t_1 in the BBSO data. Also, the secondary peak in β, which was clearly visible in the BBSO data at 20:12 UT, did not rise above the noise level in the MDI data. Thus, this peak in the BBSO data may be related to the increased image contrast (see the middle panel in Fig.5) of the ground based observations at 20:12 UT.

We can see from Figs. 4 – 7 that, in all of the cases, the amplification of the correlation length began near t_1, when β started to decrease. The growth of λ lasted until t_2 and is identified by the right vertical dotted lines in Figs. 4 – 7. In all of the cases, the maximum of β preceded the maximum of λ. The time interval between the maximum of β and the maximum of λ is denoted as $\tau_\lambda = t_2 - t_1$. We will define τ_λ to be the growth time of λ and we list its values, for all of the flares, in the 4th column of Table 2.

From Figs. 4 – 7 we estimated the relative changes, $\Delta\lambda$ and $\Delta\beta$, in percent, during τ_λ. These estimation are shown in the 4th and 5th columns of Table 1. One can see that there exists an obvious tendency for $\Delta\lambda$ and $\Delta\beta$ to grow as the X-ray flux of a flare increases.

The X9.4 flare was the only case when the value of β did not finish its rapid descent by the moment t_2, when λ was at its maximum. For this flare, we calculated $\Delta\beta \approx 81\%$ between times t_1 and 22:45 UT, when β ceased its rapid decrease. During τ_λ the value of λ increased by 46%. These relative increments of both λ and β are the largest among the four flares studied here (see Table 1).

According to the upper panels in Figs. 4 – 6, the M8.4, M8.7 and X1.6 flares increased in soft X-ray and Hα emissions and almost reached their peaks during the growth time of λ.

Table 1: Relative changes of the magnetic field parameters (correlation length, λ, scaling exponent, β, total positive magnetic flux, F^+, total negative magnetic flux, F^- and image contrast, c) during the period τ_λ of the growth of an avalanche. *The star* indicates the value of $\Delta\beta$, obtained by the ESS routine.

NOAA	Date	Flare	$\Delta\lambda,(\%)$	$\Delta\beta,(\%)$	$\Delta F^+,(\%)$	$\Delta F^-,(\%)$	$\Delta c,(\%)$
8375	Nov 5, 1998	M8.4	+13	-45	-2.5	-3.9	+4.8
0039	Jul 26, 2002	M8.7	+6.0	-63	1.0	-1.0	2.0
9661	Oct 19, 2001	X1.6	+11	-15*	4.9	0.5	4.2
6555	Mar 22, 1991	X9.4	+46	-81	+2.6	-1.0	+2.9

However, in the case of the X9.4 flare (Fig. 7), τ_λ ended less than 1.5 ± 2.9 minutes before the beginning of the enhancement of the soft X-ray emission. (Unfortunately, $H\alpha$ data are not available for this event.) This difference in timing may be due to the insufficient temporal resolution in the magnetograph data (see Fig. 7, bottom panel).

In the last three columns of Table 1 we show the relative changes of magnetic flux, $\Delta F^+, \Delta F^-$ and image contrast, Δc , (i.e. seeing and instrumental parameters) during the same period of time τ_λ. (Persistent changes are denoted by their sign). One can see that there are no systematic tendencies in the changes of the seeing and instrumental parameters, which are all less than 5% and, thus, they do not significantly effect the variations of λ and β. However, the values of $\Delta\beta$ and $\Delta\lambda$ are large enough that we are confident that they are reliable. Therefore, it is unlikely that the observed growth in λ and the decrease in β during τ_λ can be caused by changes in seeing and instrumental conditions.

4.4. Time scale comparison

Table 2 provides a comparison between different time intervals and the X-ray class of each flare.

As we mentioned above, the 3rd and 4th columns in Table 1 represent the growth time of β, τ_β, and the growth time of λ, τ_λ. Comparison between these values shows their nearly synchronous flare-to-flare changes: a decrease of τ_β is always accompanied by a shortening of τ_λ.

We defined the duration of HXR emission, τ_{dur}, as the full width at the half maximum of the time derivative of the soft X-ray emission time profile. Values of τ_{dur} are shown in the 5th column of Table 2. Comparison between the X-ray class (2nd column of Table 2) and τ_{dur} shows that, for all four flares selected for the present study, the duration of HXR emission, τ_{dur}, is inversely proportional to the peak intensity of SXR emission. This may not be a coincidence. Indeed, as it was reported by Crosby et al. (1993) and Bromund et al. (1995), there exists a statistical relationship between the peak electron energy flux, F, the total flare duration, D, and the total energy of nonthermal electrons, W: $FD \sim W^{1.18}$. This relation holds over more than 4 orders of magnitude with high correlation (the correlation coefficient is obout 0.93 (Crosby et al. 1993)). Using the HXR emission time profiles, we estimated the total energy, W, calculated for the four events. We conclude that the total energy varies within the limits which are not larger than one order of magnitude. Therefore, according to Fig. 11 in Crosby et al. (1993), the product FD also varies in the narrow range (is nearly constant), or, in other words, the peak intensity of the HXR emission,

F, is inversely proportional to its duration, D. This may be the reason for the observed inverse proportion between the X-ray class and the duration of the HXR emission for the four flares.

Comparison between the 3rd and 4th columns, on the one hand, and the 2nd and 5th columns, on the other hand, shows that, at least for the four flares under this study, the growth time of β and the growth time of λ become shorter as the X-ray class increases and the duration of the HXR emission decreases.

The 6th column in Table 2 shows the time interval, Δt, which we define to be the time between the maximum of the HXR emission and the peak of λ. The values of Δt show no systematic flare-to-flare changes and in three out of the four cases, they are nearly zero within the calculated errors.

We also estimated the time interval between the peak of λ and the maximum of the (0.5 - 4)Å GOES flux time profiles. These values, denoted as Δt^{GOES}, are shown in the 7th column of Table 2. They are close to our estimations based on the Neupert effect (see column 6).

Moreover, for the X1.6 flare we had the YOHKOH/HXR time profile, from which we calculated $\Delta t \approx -4.4$ minutes. This is very close to our estimation of -4.8 ± 2.6 min.

Thus, the parameters λ and β, as calculated for different events, vary in accordance with the other flare parameters. Namely, the duration of HXR emission and the X-ray class.

Table 2: Analyzed time intervals (in minutes): τ_β - the β growth time; τ_λ - the λ growth time; τ_{dur} - duration of the HXR emission defined as the FWHM of the time derivative of SXR emission; Δt - delay of a HXR peak relative to the maximum of λ; Δt^{GOES} - delay of the maximum of GOES (0.5 - 4)Å flux relative to the maximum of λ.

NOAA	Flare	$\tau_\beta, (min)$	$\tau_\lambda, (min)$	$\tau_{dur}, (min)$	$\Delta t, (min)$	$\Delta t^{GOES}, (min)$
8375	M8.4	33 ± 5	21± 2.5	15.0 ± 2.0	-1.8 ± 2.5	-1.0
0039	M8.7	25 ± 7	6.7 ±3.0	13.1 ± 0.7	+0.5 ± 1.8	+2.5
9661	X1.6	15 ± 3	8.1 ± 1.5	5.2 ± 0.6	-4.8 ± 2.6	-2.4
6555	X9.4	6.3 ± 3.1	3.6 ± 2.9	2.4 ± 0.5	+3.1 ± 3.9	+3.2

5. Summary and discussion

In the present study we analyzed turbulence (fractal) parameters of the longitudinal magnetic field, B_z for four major solar flares. In particular, we discussed the correlation length, λ, of the magnetic energy dissipation field and the scaling exponent, β, which characterizes the measure of intermittency (multifractality) of the B_z structure. The time variations of λ and β, during the course of a flare, were the focus of our attention. We have come to the following conclusions.

1. In all cases we found a peak in β, which was followed by a peak in λ. These two peaks were separated by the time interval, τ_λ, during which a rapid growth of the soft X-ray and $H\alpha$ flux occurred. The changes in the scaling exponent and correlation length seem to be not caused by variations of seeing and instrumental conditions.

2. The peak in β was preceded by a period of gradual growth of β, τ_β, which was longer than the time interval τ_λ.

3. The maximum of λ occurred nearly simultaneously (with the accuracy of about 2-5 minutes) with the maximum of the hard X-ray emission.

4. Based on limited examples, we conclude that the time intervales τ_β and τ_λ are inversely proportional to impulsivity ind intensity of flares.

We now address the question of what kind of processes may occur in an active region to give the observed changes in the β and λ parameters.

The increase in β during τ_β implies the strengthening of intermittency of the B_z field or the multiplication of tangential discontinuities and the accumulation of magnetic energy in the form of electric currents flowing in a variety of current sheets. In terms of percolation theory, increasing β means increasing probability, p, that an elementary volume of an active region contains a magnetic field discontinuity (the addition of trees in our example of a forest fire, see the introduction). After reaching its maximal value (i.e. $p \approx p_c$), β begins to decrease, this implies the exhausting of discontinuities in the magnetic field, or the energy release owing to reconnections (the number of unburned trees is reduced due to a quick spread of the fire over a cluster, and the energy released by the fire increases). This inference is supported by the growth of Hα and soft X-ray emissions observed during the decrease of β.

While β is decreasing, the correlation length of a magnetic energy dissipation cluster begins to rise (in other words, the characteristic size of a cluster formed by burning trees increases up to the size of the cluster before the fire, which diverges to infinity as $p \longrightarrow p_c$). Near the minimum of β the correlation length reaches its peak value. This corresponds

to the phase of the forest fire when the maximum number of trees are burning and the maximum rate of energy release is achieved. Therefore, the peaks in the time profile of the correlation length of the magnetic energy dissipation field correspond to the peaks in the magnetic energy dissipation rate, or avalanche events in the photosphere. This inference seems to be supported by the overall agreement in the time profiles between the maxima of λ and the peaks of HXR emission (peaks in energy dissipation rate in the corona).

The peak value of λ, at the moment t_2, gives an estimation of the critical size of a cluster of magnetic energy dissipation: by our calculations, $\lambda_{max} \approx 60 - 70Mm$. Note, that this value may be significantly underestimated due to the insufficient time resolution and sensitivity of the magnetic field measurements.

The observed increase in the correlation length followed by its sharp decrease may also be regarded as an avalanche in both the self-organized criticality (see review by Charbonneau et al. 2001 for references) and the logistic avalanche (Aschwanden et al. 1998) models, or regarded as a phase transition in the theory of phase transition (Feder 1988; Schroeder 2000), or regarded as a catastrophe in the theory of catastrophe. Note, that the interpretation of a large solar flare, accompanied by a filament eruption and a coronal mass ejection, as a catastrophe (a transition in the phase space) follows theoretical MHD studies (Forbes and Isenberg 1991; Lin et al. 2001).

If our interpretation of the growth of λ is correct, the conclusions of the present paper, mentioned above, may be rewritten as follows.

We can determine that during a strong solar flare an avalanche of magnetic energy dissipation events occurs, which occupies the entire active region from the photosphere to the corona, since the maximum rate of dissipation in the corona, and in the photosphere, are approximately simultaneous (maximum of λ coincides with maximum of HXR). In addition, the more abrupt is the avalanche, the stronger and/or more impulsive a flare is.

Local avalanches, with minor enhancement of the correlation length, are intrinsic properties of the non-linear dissipative processes, in particular of the SOC state (Charbonneau et al. 2001). They occur in a chaotic manner not only in space, but also in time. This may, in part, account for very jagged time profiles of λ and β, especially in the non-smoothed data (see bottom panels of Figs.4 and 6, thin lines).

For two of the flares (M8.4, Fig.4 and X1.6, Fig.6) the time resolution was sufficient to enable us to test if the time profile of a global avalanche (an avalanche related to a HXR peak) correspondences to either the exponential or the logistic avalanche models (Aschwanden et al. 1998). The logistic avalanche model predicts a Gaussian time profile, whereas the exponential model predicts a very sharp drop right after the peak. The time

profile of the avalanche of the M8.4 flare seems to correspond with the exponential model, especially when using the non-smoothed data. The X1.6 flare displays a rather Gaussian time profile of the avalanche as seen in both smoothed and non-smoothed λ time curves. Thus, either model may be applied depending on the situation. However, additional research is needed to clarify which model should be used in a particular sitiation.

If we assume that time intervals τ_β (period of enhancement of magnetic field discontinuities) and τ_λ (correlation length growth time) may be regarded in the SOC theory as the driving and avalanching time, respectively, (Charbonneau et al. 2001), we can conclude that the avalanching time for all of the events studied here was shorter then the driving time. This result is in agreement with the SOC theory. However, the observed differences between these time intervals were not as large as the SOC theory requires.

We are thankful to the BBSO observing staff for their help in obtaining the data. SOHO is a project of international coopereation between ESA and NASA. This work was supported by NSF-ATM 0076602, 0205157, 9903515 and NASA NAG5-12782 grants.

REFERENCES

Abramenko, V.I., Yurchyshyn, V.B., Wang, H., Spirock, T.J., Goode, P.R. 2002, Asprophys. J., 577, 487

Aschwanden, M.J., Dennis, B.R., Benz, A.O. 1998, Asprophys. J., 497, 972

Aschwanden, M.J., Parnell, C.E. 2002, Asprophys. J., 572, 1048

Benzi, R., Ciliberto, S., Tripiccione, R., Baudet, C., Massaioli, F., Succi, S. 1993, Physical Review E, 48(1), R29

Briscolini, M., Santangelo, P., Succi, S., Benzi, R. 1994, Physical Review E, 50(3), R1745

Bromund, K.R., McTiernan, J.M., Kane, S.R. 1995, Astrophys.J., 455, 733.

Charbonneau, P., McIntosh, S.W., Liu, H.L., Bogdan, T.J. 2001, Solar Phys., 203, 321

Consolini, G., Berrilli, E., Pietropaolo, E., Bruno, R., Carbone, V., Bavassano, B., Ceppatelli, G. 1999, in: Magnetic Fields and Solar Processes. 12-18 Sept 1999, Florence, Italy. European Space Agency SP-448, 209

Crosby, N.B., Aschwanden,M.J., Dennis, B.R. 1993, Solar Shys. 143, 275.

Datlow, D.W., Elcan, M.J., Hudson, H.S. 1974, Solar Phys.,39, 155

Denis, B.R. 1985, Solr Phys., 100, 465

Dennis, B.R., Zarro, D.M. 1993, Solar Phys., 146, 177

Feder, J. 1988, "Fractals", (New York:Plenum), Chapter 7 : Percolation

Frisch, U. 1995, "Turbulence, The Legacy of A.N. Kolmogorov", Cambridge University Press

Forbes, T. G., Isenberg, P.A. 1991, Astrophys. J., 373, 294

Georgoulis, M.K., Vilmer, N., Crosby, N.B. 2001, Astron. and Astrophys., 367, 326

Kolmogorov, A.N. 1941, C.R. Acad. Sci. USSR, 30, 301.

Krasnoselskikh, V., Podladchikova, O., Lefebvre. B., Vilmer, N. 2002, Astron. and Astrophys., 382, 699

Leka, K.D., Canfield, R.C., McClymont, A.N., Van Driel-Gesztelyi, L. 1996, Astrophys. J. 462, 547

Lin, J., Forbes, T.G., Isenberg, P.A. 2001, Journal of Geophys. Research, 106(A11), 25,053

Lin, R.P., Schwartz, R.A., Kane, S.R., Pelling, R.M., Hurley, K.C. 1984, Asprophys. J., 283, 421

Longcope, D.W., Noonan, E.J. 2000, Asprophys. J., 542, 1088

Lu, E.T., Hamilton, R.J. 1991, Asprophys. J., 380, L89

MacKinnon, A.L., Macpherson, K.P., Vlahos, L. 1996, Astron. and Astrophys., 310, L9

McIntosh, S.W., Charbonneau, P. 2001, Asprophys. J. 563, L165

Monin, A.S., Yaglom, A.M. 1975, "Statistical Fluid Mechanics", vol. 2, ed. J.Lumley, MIT Press, Cambridge, MA

Norman, J.P., Charbonneau, P., McIntosh, S.W., Liu, H.L. 2001, Asprophys. J., 557, 891

Parker, E.N. 1983, Asprophys. J., 264, 642

Parker, E.N. 1988, Asprophys. J., 330, 474

Parker, E.N. 2002, *private communication*

She, Z.H., Leveque, E. 1994, Physical Review Lett., 72(3), 336

Pustil'nik, L.A. 1998, Astrophysics and Space Science, 264(1-4), 171

Schroeder, M. R. 2000, "Fractals, Chaos, Power Laws", New York:W.H. Freeman and Company

Spirock, T.J., Denker, C., Chen, H., Chae, J., Qiu, J., Varsik, J., Wang, H., Goode, P.R., Marquette, W. 2001, in ASP Conf. Ser. 236, Advanced Solar Polarimetry Theory, Observation, and Instrumentation, ed. M. Sigwarth (San Francisco: ASP) , 65

Stolovitzky, G., Sreenivasan, K.R. 1993, Physical Review E, 48(1), R33

Vainshtein, S.I., Sreenivasan, K.R., Rierrehumbert, R.T., Kashyap, V., Juneja, A. 1994, Physical Review E, 50(3), 1823

Varsik, J.R. 1995, Solar Phys. 161, 207

Veronig, A., Vrsnak, B., Dennis, B.R., Temmer, M., Hanslmeier, A., Magdalenic, J. 2002, Astron. ans Astrophys., 392, 699

Vlahos, L., Georgoulis, M., Kluivinf, R., Paschos, P. 1995, Astron. and Astrophys., 299, 897

Wang, H., Goode, P.R., Denker, C., Yang, G., Yurchyshyn, V., Nitta, N., Gurman, J.B., Cyr, C.St., Kosovichev, A.G. 2000, Astrophys. J., 536, 971

Wang, H., Spirock, T.J., Qiu, J., Ji, H.S., Yurchyshyn, V., Moon, Y.J. 2002, Astrophys. J., 576, 497

Wang, H., Tang, F. 1993, Astrophys. J., 407, L89

Wang, T.J., Abramenko, V.I. 2000, Astron. and Astrophys., 357, 1056

Wheatland, M.S. 2000, Asprophys. J., 532, 1209

Wheatland, M.S., Sturrock, P.A., McTiernan, J.M. 1998, Asprophys. J., 509, 448

Yurchyshyn, V.B., Wang, H., Goody, P.R., Abramenko, V.I. 2000, Astrophys. J., 540, 1143